IEEE Access
Multidisciplinary | Rapid Review | Open Access Journal

IEEE ENGINEERING IN MEDICINE AND BIOLOGY SOCIETY SECTION

Received August 16, 2020, accepted September 20, 2020, date of publication October 5, 2020, date of current version October 16, 2020.

Digital Object Identifier 10.1109/ACCESS.2020.3028618

Individual Targeting Increases Control Over Inter-Individual Variability in Simulated Transcranial Electric Fields

JAN-OLE RADECKE[1], ASAD KHAN[2], ANDREAS K. ENGEL[1], CARSTEN H. WOLTERS[2,3], AND TILL R. SCHNEIDER[1]

[1]Department of Neurophysiology and Pathophysiology, University Medical Center Hamburg-Eppendorf, 20246 Hamburg, Germany
[2]Institute for Biomagnetism and Biosignalanalysis, University of Münster, 48149 Münster, Germany
[3]Otto Creutzfeldt Center for Cognitive and Behavioral Neuroscience, University of Münster, 48149 Münster, Germany

Corresponding author: Jan-Ole Radecke (j.radecke@uke.de)

This work was supported by the German Research Foundation (Deutsche Forschungsgemeinschaft, DFG) under Grant SPP 1665/SCHN 1511/1-2 to TRS and Grant SPP 1665/WO1425/5-2 to CHW.

ABSTRACT Transcranial electric stimulation (tES) induces electric fields that propagate in the brain and depend on individual anatomies. The interaction between the electric fields and individual anatomies may contribute to the heterogenous results that are commonly observed across tES studies in humans. Targeted tES is able to account for some of these individual factors by adapting the electric field to the stimulation target. Here, the effect of individually targeted tES on simulated intracranial electric fields was evaluated in head models of twenty-one participants using the finite-element method (FEM). For all participants, two individually targeted tES montages were compared to a fixed stimulation montage that was not individually optimized. For a simulated parietal stimulation target with three different orientations, individual current densities showed varying intensities near the lower limit at which physiological efficacy of electric fields can be assumed. However, targeting algorithms were able to control different electric field properties, by either maximizing the target current densities or by increasing the specificity of electric fields with respect to target location and orientation. Electric fields were constrained by individual anatomical properties, but still showed considerable variation for the given parietal stimulation target across participants. Thus, we present findings of inter-individual variability within the same cortical region to complement recent studies that showed large variation across cortical regions in a single FEM head model. Our results support the usage of individual targeting for enhancing the efficacy of tES and for elucidating the underlying mechanisms of tES. At the same time, residual variability in electric fields is suggested to be utilized for the explanation of individual differences in the tES outcome.

INDEX TERMS Individualized stimulation, multi-electrode transcranial electric stimulation, non-invasive brain stimulation, tACS, tDCS, tES.

I. INTRODUCTION

Transcranial electric stimulation (tES) is increasingly used in humans as a non-invasive tool to modulate neuronal activity in healthy and clinical samples [1]–[4]. However, a large variability regarding effects of tES on behavior and neurophysiology can be observed [5]–[9] hampering the understanding of determinants underlying tES [10]–[12]. Besides the endogenous physiological properties of the stimulation target [13], the strength, spatial distribution, and orientation of the induced electric field within the brain is affecting tES efficacy [14]–[17]. Recently, it was suggested to include simulations of the induced electric field in tES studies as a standard or even adapt the stimulation to the individual brain *a priori* [10], [18]–[20].

In typical tES applications specific cortical regions are targeted to modulate perceptual or cognitive functions with variable localization. At the same time, individual anatomies show a large variability affecting the estimated electric fields with respect to magnitude and orientation in the target [14], [15], [21]–[24]. Therefore, electric field simulation of intensity and orientation in the individual brain is of

The associate editor coordinating the review of this manuscript and approving it for publication was Carmen C. Y. Poon.

major importance to guide tES in a physiologically efficient way [25], [26]. Cortical pyramidal cells can be modeled as a summed dipole and therefore may be especially susceptible to electric fields that are oriented in parallel to the dipole orientation [25]–[29].

Methods for the evaluation of electric fields within the healthy human brain are restricted to non-invasive approaches. The finite-element method (FEM) is widely used as a realistic model for the simulation of tES-induced electric fields [23], [30]–[32] that can be utilized for the simulation of direct currents (tDCS), and the quasi-static estimation of peak electric field for alternating currents (tACS, inverted current direction at the negative peak). Based on the estimation of intracranial electric fields, the electrode placement and the applied current strength can be inversely defined to optimally target a specified brain region or dipole within the brain [33]–[37]. Using individual FEM head models, it is possible to accurately model electric fields [24], [38]–[41] and adapt the stimulation montage [22] for each participant. The stimulation parameters can be either optimized for improving the target intensity or constraining the spatial extent of electric fields [33], [34], [37].

However, previous FEM modeling studies have rarely used larger sample sizes for simulating electric fields [15], [17], [42], thus neglecting inter-individual variability. Furthermore, individually targeted tES has only been described occasionally, for example in a small sample of stroke patients [22]. Other groups defined the stimulation montage based on the topographical EEG voltage distribution in patients with Parkinson's disease [43]. This approach was previously termed naive reciprocity, as it neglects volume conduction effects for the inverse definition of the stimulation montage [36]. One previous study tested various stimulation montages before picking the one montage that showed the highest impact on a verbal task for a subsequent aphasia training [44]. FEM simulations are capable of considering volume conduction effects, in order to provide more realistic simulations and accurate targeting of tES-induced electric fields.

In the large majority of tES studies a fixed stimulation montage was applied to all participants, neglecting differences in individual anatomy. Despite the undisputed merit of this approach, it is reasonable to assume that applying the same montage to different individual anatomies leads to a high chance of misdirecting the electric field. Consequently, slightly different neural assemblies in each participant would be stimulated which would result in variable behavioral or neurophysiological tES effects. Previous publications supported the notion that electric field distributions have an impact on the actual efficacy of tES[16], [17], [45], [46]. In order to control the influence of anatomical variation, the stimulation montages can be optimized for individual stimulation targets and anatomy [33]–[37].

In the present study we simulated tES-induced electric fields in FEM-head models of twenty-one participants. We compared two optimization methods to determine individualized stimulation electrode montages: The Constrained Maximum Intensity (CMI) algorithm [47] and the Alternating Direction Method of Multipliers (ADMM) algorithm [33]. The control method was a fixed 5×1 ring-montage, which was not individually optimized. Based on a standard brain atlas, a target location was defined in parietal cortex with three orthogonal orientations. Target 1 was radial to the scalp surface (radial, RAD), target 2 was tangential to the scalp surface with an anterior-posterior orientation ($\text{tangential}_{\text{a}-\text{p}}$, TAP), and target 3 was tangential with a left-right orientation ($\text{tangential}_{\text{l}-\text{r}}$, TLR). This approach allowed to evaluate intensity and focality of the simulated electric fields and to compare them between the three methods (CMI, ADMM, 5×1). To assess the variability of parameters across subjects, realistic FEM head models were computed for a sample of twenty-one participants. In addition, we explored the parallelity of electric fields with the stimulation targets, the targeting bias as well as the heterogeneity of electric field properties across the three different target orientations.

We hypothesized that individually targeted tES montages computed with the CMI and ADMM algorithms will surpass the fixed control montage with respect to target intensity and focality, respectively. Furthermore, we assumed that targeted tES is able to address variability in individual brain structure and different target orientations by flexibly adapting electric fields with respect to the stimulation target.

II. MATERIALS AND METHODS

Optimization of stimulation electrode montages was applied, based on individual and automatically segmented six compartment FEM (6C FEM) head models using MATLAB (Natick, MA, USA), SPM12 (www.fil.ion.ucl.ac.uk/spm/), FieldTrip [48], and METH [49] toolboxes, as well as custom MATLAB-scripts (supplementary section A.). Forward solutions were computed with the open-source toolbox SimBio [50].

A. PARTICIPANTS

Twenty-one right-handed participants (12 female, 28.2 ± 4.7 years [range 20 to 37]) were included in this study. All participants reported no history of neurological or psychiatric disorders and had normal or corrected-to-normal visual acuity and hearing. Participants were reimbursed for participation and gave written informed consent prior to the experiment. The experiment was conducted in agreement with the declaration of Helsinki and the protocol was approved by the ethics committee of the Hamburg Medical Association (Ärztekammer Hamburg).

B. DATA ACQUISITION

For each subject structural T1 and T2-weighted (T1, T2) magnetic resonance (MR)-images were recorded with a 3T MR-scanner and a 64-channel head coil at an isotropic voxel resolution of $1 \times 1 \times 1$ mm (Siemens Magnetom Prisma, Erlangen, Germany). Both, T1 and T2 images were acquired

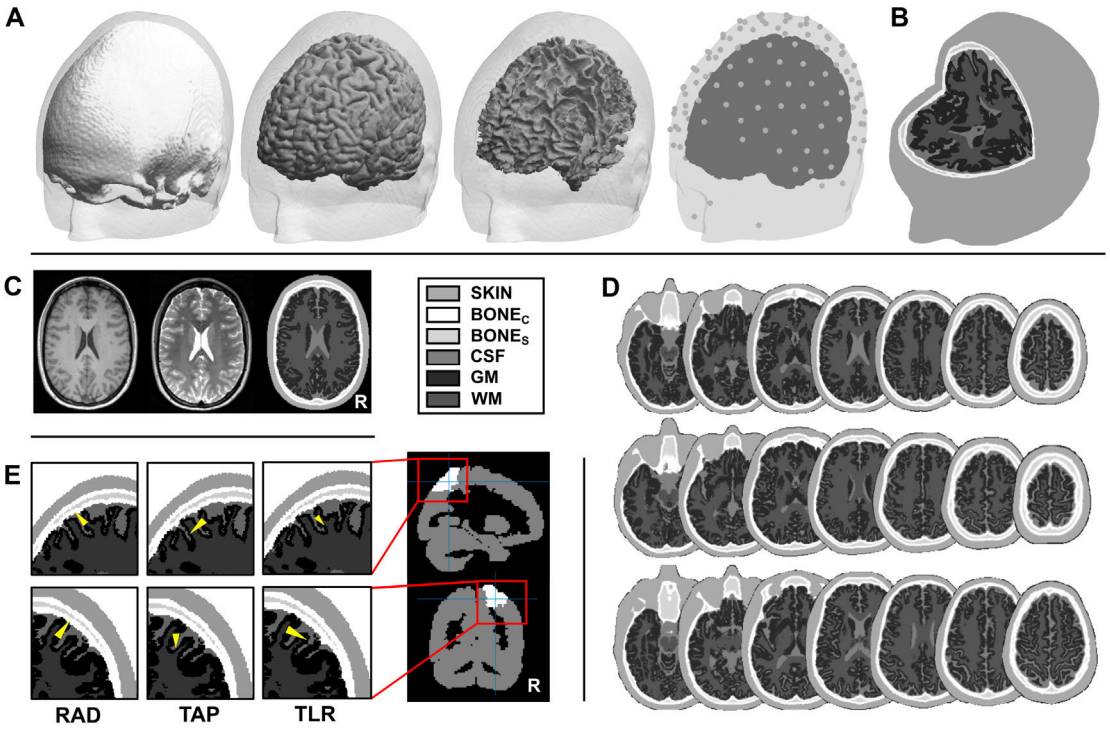

FIGURE 1. A) Isosurfaces of BONE$_C$, GM and WM compartments (from left to right), plotted within the transparent SKIN compartment for one exemplary participant. Aligned electrode positions of the 126-channel layout and, electro-oculogram electrodes, as well as fiducials are shown with respect to the GM surface and projected onto the SKIN surface. B) Complete head model showing all six compartments for the same exemplary subject (see legend for color-codes). C) Correspondence between T1 and T2 MR images with the 6C segmentation in an axial slice of the same participant shown in A) and B). D) Exemplary MRI segmentations of three participants in axial slices. E) Stimulation target orientations (yellow cones) plotted on the 6C segmented volume as a close-up of the target region of interest in right SPL. Right SPL is highlighted (white) on the overall volume that is represented by the AAL atlas. Compartments are labeled as SKIN: scalp, BONE$_C$: bone compacta, BONE$_S$: bone spongiosa, CSF: cerebrospinal fluid, GM: gray matter, WM: white matter.

with an MP-RAGE pulse sequence (T1: TR/TE/TI/FA = 2300 ms/ 2.98 ms/ 1100 ms/ 9°, FoV = 192 x 256 x 256 mm; T2: TR/TE = 3200 ms/ 408 ms, FoV = 192 x 256 x 256 mm).

C. FINITE-ELEMENT HEAD MODELS

Individual, isotropic and geometry-adapted hexahedral FEM six compartment (6C) head models were computed [23], [51]–[53]. We applied an SPM12-based [54] automatic segmentation and custom image post-processing including Boolean and morphological operations [55], [56], integrating T1 and T2 imaging data [23], [51]. These head models were utilized for the simulation of electric fields induced by tES.

Structural T1 images were non-linearly co-registered onto the T2 images. Both T1 and T2 images were then separately segmented into five compartments using SPM 12 (white matter, gray matter, bone, skin, cerebrospinal fluid). Using Boolean and morphological operations, the resulting probability maps were further processed to produce binary gray matter (GM), white matter (WM), cerebrospinal fluid (CSF), skin (SKIN), bone compacta (BONE$_C$) and bone spongiosa (BONE$_S$) compartment masks (Fig. 1A to D).

In contrast to other available automated segmentation tools [30], [55], BONE$_S$ was included in the model. Due to higher conductivity of BONE$_S$, compared to BONE$_C$, the current flow is redirected from an otherwise radial flow through the low-conductive BONE$_C$ [23]. This effect might lead to an increased outspread of the electric field across the underlying cortical surface and counteracts the insulating effect of BONE$_C$ in regions of thick skull, especially in dorsal skull regions [14]. Although the effect of BONE$_S$ is negligible with respect to the current density in the directly underlying cortex [14] it yields a complex effect on the overall cortical current density and on the orientation of the current [14], [23]. To dissociate BONE$_C$ and BONE$_S$, the binary bone mask was eroded and thresholded, based on the original T2 probability maps [23], [51]. In order to integrate information of the different binary compartment masks into one volume, ambiguous labels were removed, while fixating BONE$_C$ and BONE$_S$ in order to alleviate or avoid leakage artifacts [57], [58]. Missing tissue labels were interpolated iteratively using the nominal information from neighboring voxel labels, implemented in custom MATLAB software.

The head volume was transformed to the CTF coordinate system (principal axes are going through fiducial points at the nasion and the bilateral tragi, X-axis towards nasion, Y-axis towards the left tragus, Z-axis towards the vertex). The lower

third of the volume was cut off to reduce the overall size of the head model. Finally, a geometry-adapted hexahedral finite-element mesh was computed for the 6C head model volume of each subject. The geometry-adaptation was calculated using a node shift of 0.33 to ensure that the inferior angles at element vertices remain convex and the Jacobian determinant in the FEM computations remains positive. Tissue conductivities were defined as 0.33 (GM), 0.14 (WM), 1.79 (CSF), 0.43 (SKIN), 0.025 ($BONE_S$) and 0.007 ($BONE_C$), as well as 1.4 S/m for the electrodes [23], [33].

D. STIMULATION ELECTRODES AND SIMULATED TARGETS

Individual electrode positions from 126-channel EEG caps (EasyCap, Herrsching, Germany) were optically registered (Xensor, ANT Neuro, Hengelo, The Netherlands) and averaged to a standardized template across all subjects to eliminate potential measurement errors from the individual electrode registration. Template electrode positions were aligned to the individual head models, directed by the fiducial points (nasion and bilateral tragi, Fig. 1A). Electrodes were simulated using a point electrode model [59], by projecting the aligned electrode position to the closest FEM node on the scalp surface. The overall stimulation current was scaled to 2 mA. In order to compare the different optimization and the control methods, the number of stimulation electrodes was fixed to $n = 6$ for each individual stimulation montage (supplementary section B.).

Stimulation targets were defined in the right superior parietal lobule (SPL) as a region of interest, based on the AAL brain atlas (Automated Anatomical Labeling) [60]. SPL was shown to be part of the dorsal frontoparietal attention network [61] and parietal cortex represents a realistic stimulation target for various tES applications [7], [62]. For each head model, individual 3D-grids (5 mm), sampling the combined CSF, GM and WM compartments were defined in CTF space. By linear normalization of the individual T1 images on the MNI152 template brain (Montreal Neurological Institute, Montreal, Canada), the individual grids were warped into MNI space to determine the average coordinate of all grid points within the right SPL in MNI-space. Using the inverse of the transformation matrix, target coordinates were then warped backed into the individual CTF coordinate system and projected on the closest GM node of the individual head models. Finally, three orthogonal target orientations were simulated with respect to the individual scalp surface (Fig. 1E) to evaluate the reliability of electric fields for the two targeting algorithms and the control method across target orientations. One orientation was defined as radial to the scalp surface. Two tangential target orientations were computed along the anterior-posterior axis and along the left-right axis, respectively.

E. INVERSE OPTIMIZATION OF STIMULATION MONTAGES AND SIMULATION OF ELECTRIC FIELDS

We compared two individually targeted tES montages with a fixed control montage, employing the adjoint method [52] implemented in the SimBio toolbox (SimBio Development Group) for simulation of intracranial electric fields.

We computed matrix A (Eq. 3) which is symmetric to the lead field in EEG inverse problems due to Helmholtz' reciprocity [36], [52]. Likewise, matrix A can be used to find the best possible weighting of current at the stimulation electrodes s_{max} under a defined set of constraints. Matrix A was computed by combining the individual m electrode positions and the 6C FEM head models with n nodes (3.64 ± 0.29 million nodes [range 3.02 to 4.20 million]). Matrix A holds the forward model vectors $a_n(r_n)$ at r_n, which is the n_{th} node of the FEM model, while assuming a fixed current s_m applied to every combination of a fixed reference electrode and the m_{th} electrode of the given 126-channel layout. The current density vector field j at each node r_n for a given stimulation montage is determined by the linear combination of the weighted current s (including the reference electrode) applied to any combination of the m electrodes as a function of A:

$$j = As \tag{1}$$

with

$$j = \begin{bmatrix} j(r_1) \\ j(r_2) \\ \vdots \\ j(r_n) \end{bmatrix},$$

$$A = \begin{bmatrix} a_1(r_1) & a_2(r_1) & \dots & a_m(r_1) \\ a_1(r_2) & a_2(r_2) & \dots & a_m(r_2) \\ \vdots & \vdots & \ddots & \vdots \\ a_1(r_n) & a_2(r_n) & \ddots & a_m(r_n) \end{bmatrix},$$

and

$$s = \begin{bmatrix} s_1 \\ s_2 \\ \vdots \\ s_{m-1} \\ -\sum s_m \end{bmatrix}$$

The applied optimization algorithms compute the optimal stimulation montages by either maximizing the target current density or by applying additional constraints to the spatial extent of the electric field, in order to balance stimulation intensity and focality.

1) THE CMI ALGORITHM

In the present study, we used a modified version of the Maximum Intensity algorithm [34], the Constrained Maximum Intensity (CMI) approach [47]. The CMI is expressed as:

$$s_{max} = \min_s j_t Cs - \lambda \|s\|_2 \quad \text{subject to } \|s\|_1 \le 2i_{Total}, \text{ and } \|s\|_\infty \le i_{Limit}, \tag{2}$$

with

$$C = [a_1(r_n), a_2(r_n), \dots, a_m(r_n)],$$

where n_t denotes the index of the target node and j_t the target current density vector. C is the submatrix from A that reflects the mapping of the electrode currents to the current density at the target vector. In this approach the maximum current applied to each electrode can be limited by a maximum norm constraint [22]. Additionally, the applied current is distributed among stimulation electrodes by introducing the L2-norm [47]. In the present simulations, we chose $\lambda = 250$ to slightly distribute the injected currents across electrodes (supplementary section B.). $i_{Total} = 2$ mA was set to fulfill the safety constraint and $i_{Limit} = 0.95$ mA to enforce a distribution of electrode currents and reduce the theoretical tactile perception of the stimulation under each electrode. In a two-step procedure, the stimulation montage was fixed to six electrodes for each individual stimulation montage.

2) THE ADMM ALGORITHM

The Alternating Direction Method of Multipliers (ADMM) algorithm maximizes the current density in the stimulation target Ω_t, while controlling the current densities in the remaining non-target volume conductor Ω. As described in detail by Wagner and colleagues [33], we considered an optimal control problem for a Laplace equation with Neumann boundary conditions with control and point-wise gradient state constraints. For numerical solution of the corresponding discretized problem the alternating direction method of multipliers was employed:

$$s_{max} = \min_{s} \int_{\Omega_t} < As, j_t > dx - \alpha \int_{\partial\Omega} s^2 \Omega dx - \beta \|s\|_{1(\partial\Omega)} \quad \text{subject to } w|As| \leq \varepsilon \tag{3}$$

Herein, w reflects the weighting matrix that mediates between current densities in target and non-target regions. The parameter ε from the gradient state constraint reflects the upper bound of current densities in non-target regions and was set to 0.5 to enable focality of the solution. The L2-regularization parameter α penalizes the energy of the applied current pattern. The L1-regularization parameter β is used to minimize the number of active electrodes. We set both of these parameters to 0.0001 (elastic net) in order to guarantee a unique minimizer. A two-step procedure ensured the fixed number of electrodes: After an initial optimization, the six electrodes with the maximal current weighting were selected. The applied currents were balanced, while separately preserving the optimized current weightings for anodes and cathodes, respectively. Results from pilot simulations showed reasonable electrode montages and current densities using this adapted version of the ADMM (supplementary section B.), while meeting the requirements of a fixed number of electrodes. i_{Total} was scaled to 2 mA.

3) THE FIXED CONTROL MONTAGE

Fixed montages for typical tES applications, can be constructed by placing one central small electrode radially over the estimated stimulation target and placing four small electrodes with inverted polarity in a ring around the central electrode (4×1) [32]. This approach was shown to yield reasonable current densities, while limiting the spatial extent of the electric field, compared to tES using large and distant patch electrodes. In line with this procedure, we defined a fixed control stimulation montage with five small electrodes, arranged in a ring (5×1; considering the electrode layout in the current experiment) around a small center electrode that is placed closest to the radial projection of the target coordinate to the scalp, for the MNI152 template (Montreal Neurological Institute, Montreal, Canada). The defined 5×1 standard montage was applied to all individuals in order to simulate a normative stimulation montage design that was not individually optimized. The distance between the center-electrode and surrounding electrodes was optimized manually, with respect to intensity and spatial extent of the stimulation. This definition of the control montage mimics the conventional approach of tES applications which commonly neglects individual anatomy and orientation of the stimulation target.

F. QUANTIFICATION AND STATISTICAL ANALYSIS OF SIMULATION RESULTS

Current densities [A/m^2] were computed for each node of the FEM head model. No significant leakage artifacts were revealed by the modeling results of current flow across participants and target orientations [57], [58]. Current density vectors were corrected for the angular deviation between the stimulated field and the target vector orientation. Stimulation intensity was defined as the 0.95 percentile of values within 5 mm distance to the target vector. The highest intensity is not necessarily centered at the stimulation target, but a bias of the electric field orientation can be observed. In order to quantify this bias and the spatial extent of the electric field, taking the bias into account, the 0.95-percentile was computed as a function of the Euclidean distance to the stimulation target. The function was normalized with respect to the maximum value. The bias of the electric field was quantified as the distance (in mm) between the maximum of the normalized function and the target. Spatial extent was quantified as the distance (in mm) at 50% area under the curve of the normalized function. In addition, the parallelity between the target orientation and the target current density vector orientation was quantified as the absolute of the dot product between the two orientation vectors (range: 0 to 1, with 0 = orthogonal orientations and 1 = parallel/anti-parallel orientations). Thereby, the alignment of the electric field orientation (within the stimulation target) with the target orientation was estimated.

Repeated measures 3×3-ANOVAs were computed to compare the effect of three different stimulation methods (ADMM, CMI, 5×1) and three different target orientations (radial, tangential$_{a-p}$, tangential$_{l-r}$) for stimulation target intensity, spatial extent, bias and parallelity, separately.

The reliability of each method was assessed by quantifying the heterogeneity of the simulated electric fields across the three different target orientations, with respect to both target current density and spatial extent of electric fields (see sup-

plementary section C. and D.). Target current densities and spatial extent values were normalized across all methods and target orientations, respectively. Heterogeneity was computed as the subject-wise sum of pair-wise Euclidean distances between the normalized $\begin{bmatrix} Intensity \\ Focality \end{bmatrix}$-vectors for the three target orientations (i.e. distances were computed for RAD-TAP, RAD-TLR and TAP-TLR and summed for each method and subject).

A repeated-measures ANOVA was computed to compare the effect across the three different stimulation methods (ADMM, CMI, 5 × 1) for the heterogeneity parameter.

In general, Greenhouse-Geisser correction was applied, if the sphericity assumption was violated. Follow-up paired samples t-tests were computed and p-values were corrected for multiple comparisons using the Bonferroni-Holm method [63]. Non-parametric Spearman correlations were computed to describe the relationship between intensity and spatial extent for each method and target direction, separately. Sample means and standard deviations were reported, if not indicated otherwise. Significance level was set to $\alpha = 0.05$ and effect sizes η_p^2 and r were reported, respectively. Corrected p-values are reported if not indicated otherwise. Detailed information on statistics is provided in Table 1 to 3 (also see supplementary section C.).

III. RESULTS AND DISCUSSION

We simulated current densities induced by individually optimized tES montages in realistic 6C FEM head models of twenty-one participants. A fixed control montage was compared with two individually targeted stimulation montages optimizing predominantly stimulation intensity or focality. Unilateral targets with three different vector orientations were positioned in the right SPL. We show that individual optimization allows to control variability due to individual structure, as well as target location and orientation. Although this effect was reliable across the sample, the results also reveal that even optimized electric fields are limited by individual anatomical properties. Taken together, the present results substantiate the need for integrating individual electric field simulations with tES applications.

A. INDIVIDUAL TARGETING ADAPTS TO INDIVIDUAL STIMULATION REQUIREMENTS

Electrode montages provided by the ADMM and CMI algorithms showed the expected variation across subjects (see Fig. 2). By recruiting more than one central stimulation electrode, the ADMM flexibly corrected the current flow, if the radial targets did not project directly on a stimulation electrode at the scalp surface. For tangential targets, ADMM provided two antagonistic electrode clusters that were placed close to one another along the target direction in order to preserve focality of the stimulation. For the CMI algorithm and the tangential target orientations, two similar electrode clusters were located with increased distance to one another, compared to the ADMM montages. In general,

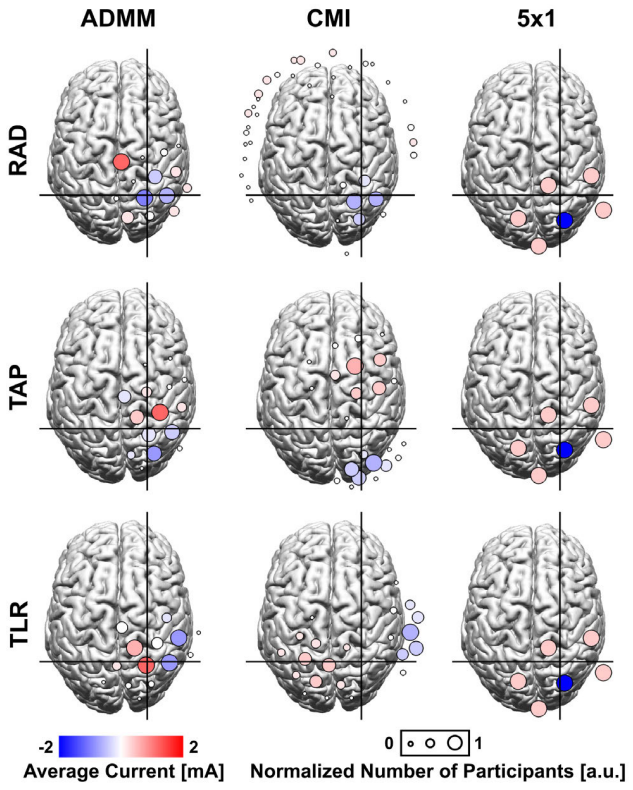

FIGURE 2. Three-dimensional illustration of the grand average electrode montages that were derived from the focality-optimizing ADMM, intensity-optimizing CMI and a 5 × 1 fixed control montage. A template cortical surface (FieldTrip) is plotted, viewed from the top. For each method (from left to right: ADMM, CMI, 5 × 1) and target orientation (from top to bottom: radial (RAD), tangential$_{a-p}$ (TAP), tangential$_{l-r}$ (TLR)) the electrode sizes reflect the number of participants for whom the respective electrode was part of the montage. Large circles illustrate that for all participants this particular electrode was part of the montage. Smaller circles illustrate fewer usages of the particular electrode. The color of the circles shows the average current applied to the electrode across participants. Red and blue colors indicate that this particular electrode rather had the same polarity across subjects, as well as their relative weighting. White electrodes indicate either small current applied to the electrode or variable electrode polarity across participants. Electrodes that were not part of the resulting electrode montages were omitted, respectively. Crosshairs indicate the average location of the stimulation target in SPL. Control 5 × 1 montages show no variability in the electrode montages and uncorrected current densities, but are depicted here for illustrative reasons.

both optimization approaches made extensive use of the high-density electrode layout in order to address the requirements of individual anatomy and variations in target location and orientation.

Furthermore, in practice the close distance of electrode positions in a high-density electrode layout enables the stimulation current to be split among a number of small electrodes [32]. Thus, still at increasing stimulation intensity, skin sensations can be minimized, while preserving a minimal loss of focality of the electric field. The different electrode montages resulted in distinct properties of the induced electric fields with respect to parallelity (section III.B, Fig. 3) intensity, spatial extent, as well as reliability of the electric fields (sections III.C-E, Fig. 4). Exemplary electrode montages and the resulting electric fields for one subject showed

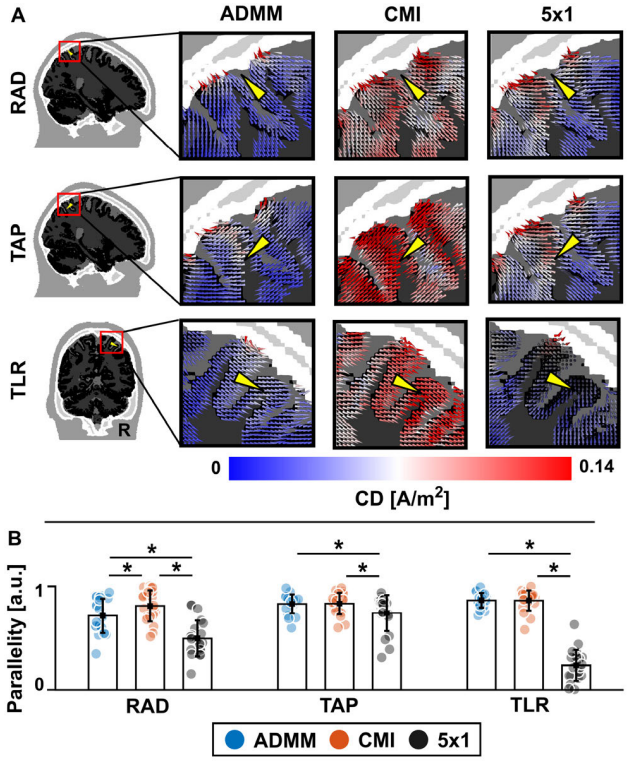

FIGURE 3. A) Close-up of the finite-element vector field and target vectors for all methods (from left to right: ADMM, CMI, 5 × 1) and target orientations (from top to bottom: radial, tangential$_{a-p}$, tangential$_{l-r}$) in one exemplary participant. To optimally depict the field alignment with the target vector orientation, sagittal slices are presented for the radial and tangential$_{a-p}$ targets and coronal slices are presented for the tangential$_{l-r}$ target. Vector fields were nicely aligned for both ADMM and CMI with varying spatial extent of the uncorrected current densities and varying maximal current densities. Control 5 × 1 montages showed no variability in the electric field, but clear misalignments of the target vector and the electric field were obvious, compared to the targeted electric fields and especially for the tangential$_{l-r}$ target orientation (also see supplementary section F). B) On group level, parallelity (mean ± standard deviation; SD) was significantly smaller for the 5 × 1 control montage across all target orientations and showed large differences across target orientations for the 5 × 1 control montage. * indicate $p < 0.05$.

similar patterns as described for the sample (Fig. 5). The present data supports the conclusion that the utilization of high-density electrode layouts for the individual optimization of tES montages [37] is beneficial, in order to allow the adaptation to the stimulation target, under consideration of the individual anatomy of the participants.

B. TARGETED ELECTRIC FIELD ORIENTATIONS

As expected, current density vectors resulting from the targeted tES montages were well aligned with the target orientation (Fig. 3 and 5; Table 1) [33], [34], [47]. In contrast, the control montage failed to reliably comply with the three target orientations. A significant interaction effect of the factors *method* and *target orientation* was observed (Table 2) and follow-up *t*-tests revealed a consequently reduced parallelity for the electric fields, induced by the 5 × 1 montage, compared to the optimized montages for all target orientations (Table 3). In addition, for the radial orientation, CMI showed significantly higher parallelity, compared to the ADMM (Fig. 3B).

TABLE 1. Descriptive data for the bias and parallelity of the current density vector field, with respect to the stimulation target. Target orientations are labeled as RAD: radial, TAP: tangential$_{a-p}$ and TLR: tangential$_{l-r}$. Mean ± standard deviation is reported.

	BIAS [mm]	PARALLELITY [a.u.]
ADMM$_{RAD}$	10.7 ± 4.3	0.71 ± 0.17
ADMM$_{TAP}$	8.1 ± 3.0	0.83 ± 0.09
ADMM$_{TLR}$	9.3 ± 3.3	0.86 ± 0.07
CMI$_{RAD}$	26.4 ± 21.5	0.81 ± 0.15
CMI$_{TAP}$	10.7 ± 7.3	0.83 ± 0.11
CMI$_{TLR}$	10.5 ± 6.3	0.86 ± 0.10
5x1$_{RAD}$	24.3 ± 4.8	0.50 ± 0.17
5x1$_{TAP}$	10.0 ± 3.5	0.74 ± 0.17
5x1$_{TLR}$	23.6 ± 6.4	0.24 ± 0.15

Cortical pyramidal cells might be especially susceptible to electric fields that are oriented in parallel to the target orientation, and thus also to changes in the orientation of the electric field [25]–[29]. Although the specific role of the electric field orientation for tES-induced electric fields in humans is not yet resolved, in theory, an electric field that is orthogonal to a physiological dipole is not expected to exert an effect. Consequently, the alignment of tES-induced electric fields with the stimulation target is physiologically relevant. In the present study we explored the alignment of targeted electric fields compared to the alignment of the 5 × 1 control montage. Due to the deviating parallelity of electric fields in the control montage, corrected current densities are reported, considering the misalignment of the electric field vector and the respective target orientation.

The present study further indicates the importance of considering the target orientation, independent of target depth. Radial targets showed overall lower target current densities, compared to both tangential orientations for ADMM and CMI (Fig. 4; supplementary section D.) [34], while no difference was observed between the two tangential orientations, respectively. In the present study, stimulation targets were located in intermediate sulcal depth for all target orientations. Previous simulations of targeted tES investigated the effect of target depth, comparing superficial radial targets with intermediate or deep tangential targets [33], [34]. Herein, current densities were reduced, with increasing depth of the stimulation target [33]. However, these studies were inconclusive on how targeted stimulation can cope with varying target orientations, independent of target depth. We conclude that - in intermediate depth of the simulated parietal target in the present experiment - targets with tangential orientations would be stimulated with a relatively higher current density, compared to radial targets, across individual participants. Nevertheless, the same conclusion does not necessarily hold for other stimulation targets in deeper [64], [65], or more superficial cortical areas, or other regions of the brain, other than parietal cortex [66].

C. TARGETED STIMULATION INTENSITIES

In the present study, target current densities ranged from 0.007 A/m^2 (5 × 1, tangential$_{l-r}$) to 0.176 A/m^2 (CMI, radial).

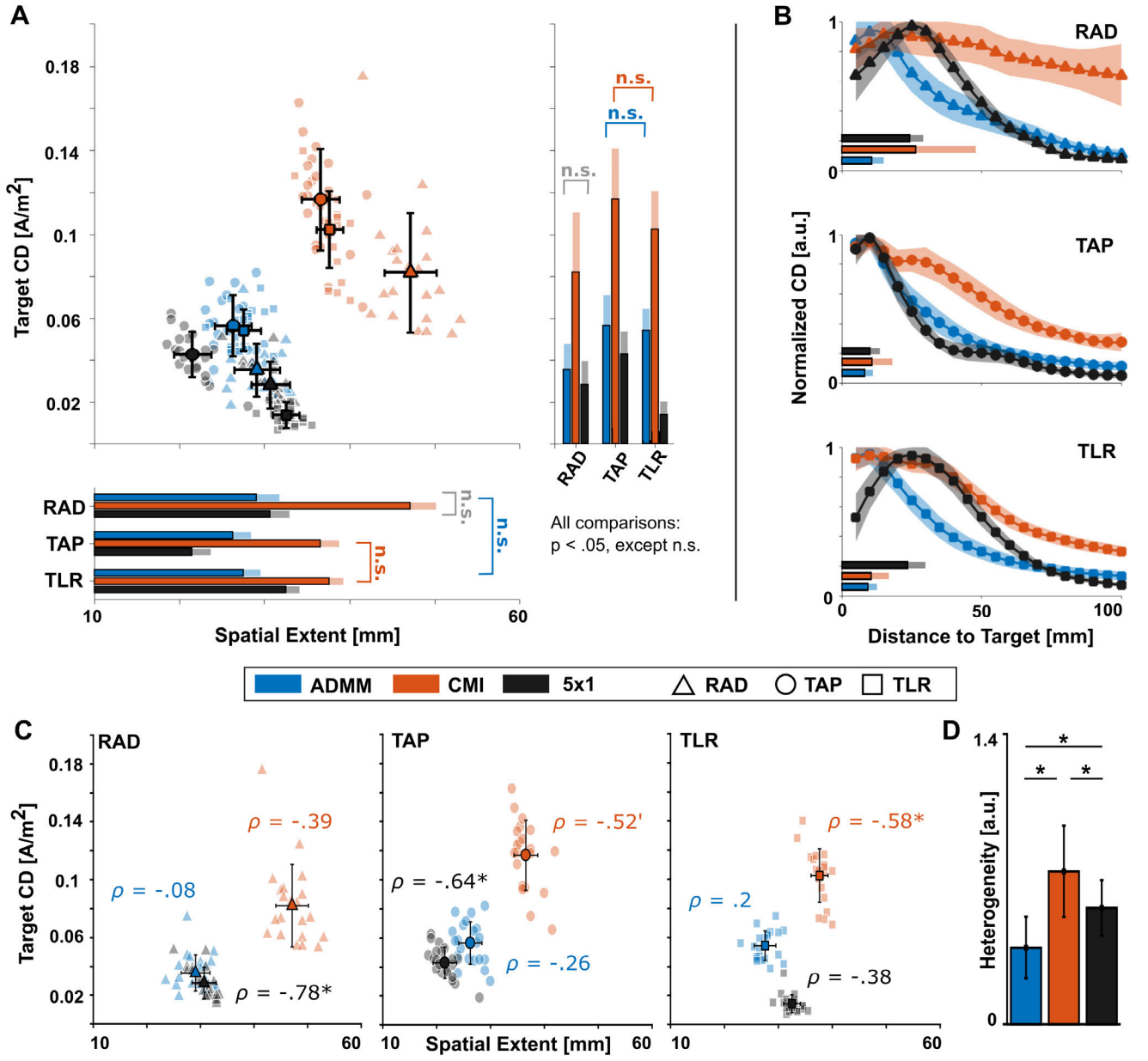

FIGURE 4. A) Target current densities (CD) plotted against the spatial extent for every method and target orientation. Group averages are represented by colored symbols with black edges (mean ± SD). Single-subjects are plotted in light colors. Bar graphs illustrate the descriptive average target CD and spatial extent, respectively. Light colored stacked bars represent the SD. Statistical analysis, comparing target current densities and spatial extent reveals significant differences in both parameters. Results are reported in detail in Table 2 and 3. *n.s.* indicates *not significant* ($p > 0.05$). B) Line plots represent averages of individually normalized current densities as a function of distance to the target vector for each of the applied methods and target orientations (from top to bottom: radial, tangential$_{a-p}$, tangential$_{l-r}$), illustrating the distribution of the electric field, independently of the intensity. Colored bars indicate bias (mean ± SD) of the targeted electric fields (see Table 1). C) Non-parametric Spearman correlations were computed and revealed negative relations of target current densities and spatial extent in some method-target combination. In other words, some subjects showed an increased profile of the electric field parameters both being more intense and more specific, compared to other subjects, even for the targeted CMI. D) Heterogeneity (mean ± SD) for each ADMM, CMI and 5 × 1 control montage across stimulation target orientations. Small heterogeneity reflects the reliability of the respective method across different stimulation target orientations (high values indicate heterogeneity; low values indicate homogeneity). ' indicate $p < 0.1$ and * indicate $p < 0.05$.

These observed target intensities fit into the range of previously reported FEM simulation results (Fig. 4A, supplementary section E.) [14], [23], [33], [34], [42], [67]. Statistical analysis of target current densities revealed a significant interaction between the two included factors method and target orientation (Fig. 4A, Table 2). Across methods, CMI consistently showed significantly higher target current densities, compared to the ADMM and 5 × 1, as revealed by follow-up *t*-tests (Table 3, see supplementary section D.). For both tangential target orientations, ADMM showed increased

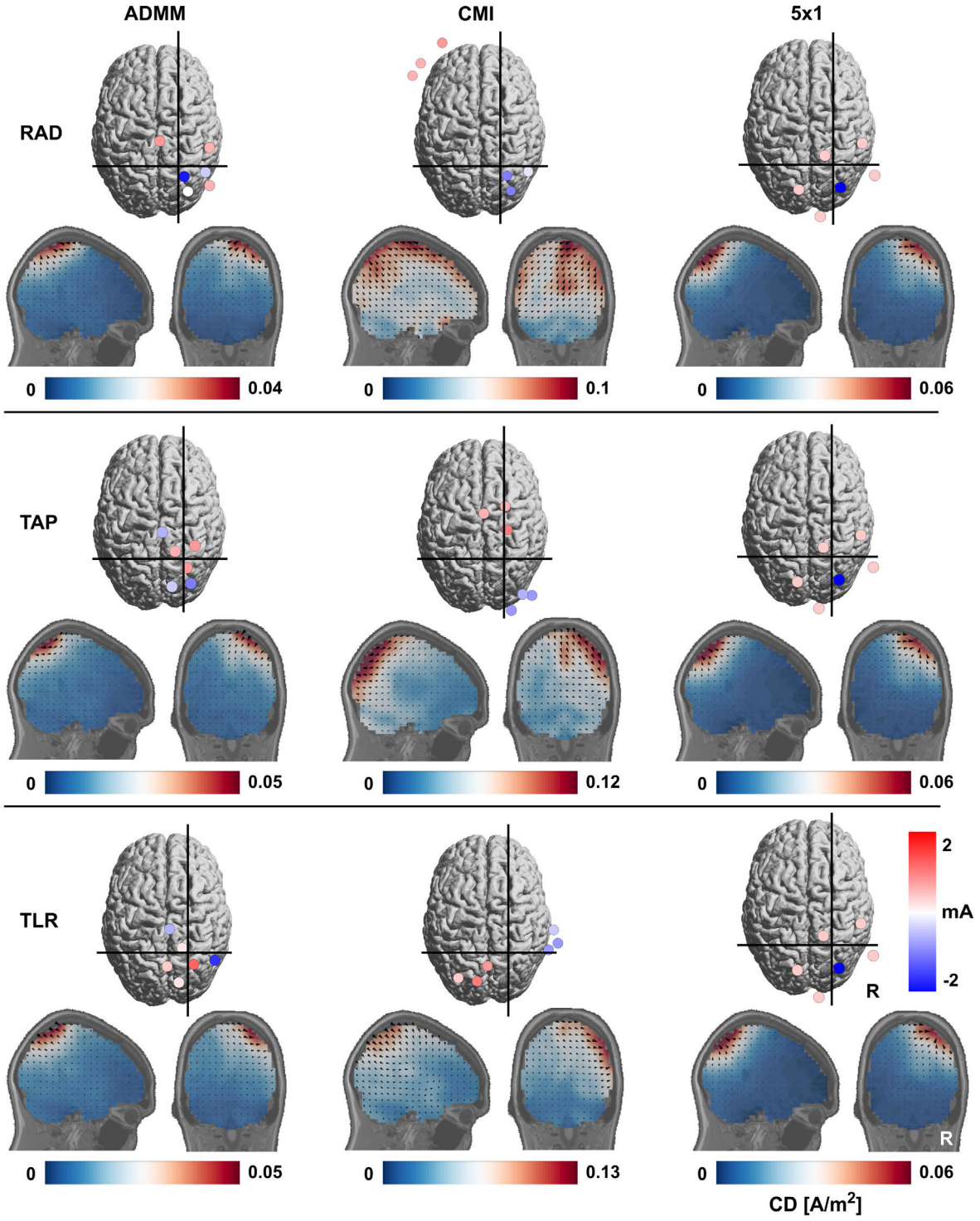

FIGURE 5. Three-dimensional illustration of electrode montages that were derived from the focality-optimizing ADMM, intensity-optimizing CMI and a 5 × 1 fixed control montage for one exemplary participant. The individual cortical isosurface is plotted, viewed from the top. For each method (from left to right: ADMM, CMI, 5 × 1) and target orientation (from top to bottom: radial, tangential$_{a-p}$, tangential$_{l-r}$) the electrodes are depicted by circles of the same size. The color of the circles reflects the current applied to the respective electrode. Sagittal and coronal slices through the target vector are presented for each electrode montage at the target location. Uncorrected intensities were interpolated on an individual 5 mm grid including GM, WM and CSF and were plotted on top of the individual T1 image. To illustrate the current density distribution across the brain, custom scales were chosen for each method and target orientation. Three-dimensional vector fields were projected to the respective two-dimensional plane, scaled by the uncorrected current density and plotted on a sparse grid. Vector fields reflect the alignment of targeted tES montages to the target vector orientation (see Fig. 3). Control 5 × 1 montages show no variability in the electrode montages and uncorrected current densities, but are depicted here for illustrative reasons.

TABLE 2. Results of ANOVA's testing differences in target intensity, spatial extent, parallelity and bias. Repeated measures ANOVA's were computed across methods (ADMM, CMI, 5 × 1) and target orientations (radial, tangential$_{a-p}$, tangential$_{l-r}$). Significant main effects for both factors and a first order interaction effect were revealed. * indicate $p < 0.05$.

		p	F_{df}	df	η_p^2
INTENSITY	METHOD	< .001	509.8 *	2, 40	0.96
	TARGET ORIENTATION	< .001	21.1 *	2, 40	0.51
	METHOD x TARGET ORIENTATION	< .001	19 *	2.5, 49.9	0.49
SPATIAL EXTENT	METHOD	< .001	900.1 *	2, 40	0.98
	TARGET ORIENTATION	< .001	180.6 *	2, 40	0.90
	METHOD x TARGET ORIENTATION	< .001	70.5 *	2.6, 51.3	0.78
BIAS	METHOD	< .001	17.81 *	1.2, 23.9	0.47
	TARGET ORIENTATION	< .001	22.74 *	2, 40	0.53
	METHOD x TARGET ORIENTATION	.001	11.22 *	1.5, 30.5	0.36
PARALLELITY	METHOD	< .001	372.8 *	2, 40	0.95
	TARGET ORIENTATION	.003	8.3 *	1.5, 30.6	0.29
	METHOD x TARGET ORIENTATION	< .001	47.3 *	2.5, 50.9	0.70

TABLE 3. Follow-up t -tests of the method x target orientation interaction showing differences in target intensity, spatial extent, bias and parallelity across methods. Target orientations are indicated as RAD: radial, TAP: tangential$_{a-p}$ and TLR: tangential$_{l-r}$. * indicate $p < 0.05$.

		INTENSITY		SPATIAL EXTENT		BIAS		PARALLELITY	
		t_{20}	r	t_{20}	r	t_{20}	r	t_{20}	r
ADMM$_{RAD}$	**CMI$_{RAD}$**	-12.32 *	0.94	-21.04 *	0.98	-3.53 *	0.62	-3.06 *	0.56
ADMM$_{RAD}$	**5x1$_{RAD}$**	2.46	0.48	-2.32	0.46	-9.79 *	0.91	5.89 *	0.80
CMI$_{RAD}$	**5x1$_{RAD}$**	9.70 *	0.91	19.44 *	0.97	0.43	0.10	8.40 *	0.88
ADMM$_{TAP}$	**CMI$_{TAP}$**	-16.33 *	0.96	-28.08 *	0.99	-1.86	0.38	-0.23	0.05
ADMM$_{TAP}$	**5x1$_{TAP}$**	4.99 *	0.74	8.22 *	0.88	-2.61	0.50	2.70 *	0.52
CMI$_{TAP}$	**5x1$_{TAP}$**	20.52 *	0.98	23.78 *	0.98	0.51	0.11	3.17 *	0.58
ADMM$_{TLR}$	**CMI$_{TLR}$**	-14.54 *	0.96	-24.55 *	0.98	-1.16	0.25	0.15	0.03
ADMM$_{TLR}$	**5x1$_{TLR}$**	14.75 *	0.96	-9.49 *	0.90	-10.26 *	0.92	18.29 *	0.97
CMI$_{TLR}$	**5x1$_{TLR}$**	23.76 *	0.98	12.71 *	0.94	-6.66 *	0.83	18.44 *	0.97

target current densities, compared to the 5 × 1 control montages, but not for the radial orientation, indicating the practicality of standard montages for some specific applications.

In previous studies, *in vitro* and *in vivo* recordings reported subthreshold modulation of neuronal activity that was induced by electric fields with peak intensities at 0.2 to 0.5 V/m (approx. 0.066 to 0.165 A/m^2) using alternating current stimulation [68]–[70]. In line with previous modeling results [14], [23], [33], [34], [67], the present results indicate that tES is acting at the lower end at which electric fields were reported to modulate neural activity (see Fig. 4) [68]–[71]. Still, due to varying tissue conductivities[24], [51], [72], [73], effects of network electric activity [68], [71] and the effective state of the stimulated neuronal population in humans [74], [75], already relatively weak electric fields might modulate neuronal activity in specific cases. Using the CMI algorithm, the target current densities were increased for the given parietal stimulation target, compared to ADMM and the 5 × 1 control montages (Fig. 4, Table 3). ADMM showed increased target current densities for the tangential stimulation targets, compared to the 5 × 1 control. By increasing the target current density, the probability is increased that individual electric fields will take physiological effect within the stimulation target [71], [76]. Taken together, the present results substantiate the importance of targeting the electric field with respect to the stimulation target in order to maximize the physiologically effective electric field intensity. Although it is not yet resolved to what extent the electric field strength is affecting the behavioral tES outcome, preliminary results indicate its physiological relevance [16], [17].

D. TARGETED ELECTRIC FIELD DISTRIBUTION AND BIAS

Evaluation of the spatial extent across methods and target orientations revealed a significant interaction effect (Table 2). ADMM-optimized electric fields were characterized by small spatial extent (Fig. 4A), i.e. maximal current densities in close vicinity to the target and steep slopes of current density as a function of distance to the stimulation target (Fig. 4B). No difference in intensities and spatial extent of electric fields was revealed between ADMM and 5 × 1 montages for the radial orientation by follow-up t-tests (Table 3). At the same time, electrode montages computed with the CMI consistently showed the largest spatial extent of electric fields across all target orientations compared to ADMM and the 5 × 1 control montage. With respect to the tangential$_{a-p}$ target, 5 × 1 montages showed significantly reduced spatial extent of the simulated electric fields, compared to both optimized methods. The spatial extent of ADMM electric fields was reduced for the tangential$_{l-r}$ orientation, compared to both CMI and the 5 × 1 control.

In addition to the spatial extent of electric fields, an interaction effect of the factors method and target orientation was

revealed for the targeting bias (Table 2). ADMM consistently resulted in small targeting bias of the electric field, with respect to the stimulation target (Fig. 4B, Table 1). Although CMI showed a small bias for both tangential target orientations comparable to ADMM. The CMI-derived electric fields for the radial orientation showed a high bias (26 mm) and descriptively high inter-individual variability (Table 1). Electric fields derived from the 5 × 1 montages showed a strong bias of up to 24 mm for the radial and tangential$_{l-r}$ orientations, compared to the ADMM-derived electric fields (Fig. 4B, Table 1 and 3). For the tangential$_{a-p}$ target orientation the electric field bias of the 5 × 1 control montage was significantly reduced compared to ADMM (which showed a descriptively small bias already).

In sum, we conclude that ADMM was able to accurately direct the electric field to the stimulation target, while adapting to different target orientations and with reliable spatial extent of electric fields. The electrode montages for CMI and the radial orientation were widely distributed across the scalp (Fig. 2) inducing widely distributed electric fields (Fig. 4A and 5) which also resulted in an increased bias across subjects, however, only for the CMI and the radial orientation. For the tangential targets CMI achieved an accurate targeting, although the electric fields were extended across the brain compared to ADMM and 5 × 1 control montages. The 5 × 1 control montage showed quite focal electric fields across the different target orientations. However, for the radial and the tangential$_{l-r}$ targets the high bias compromised the spatial extent of the electric fields with respect to the stimulation target (and thereby also the target current densities). It has to be noted that for the tangential$_{a-p}$ target the 5 × 1 montage resulted in reasonable focality and only a small bias (in addition to a reasonable alignment of the electric field with the target orientation; Fig. 4A and B). Therefore, it can be assumed that for some situations a standard montage can result in potentially effective electric fields. However, with respect to physiologically effective target current densities that can be assumed to modulate neuronal activity [68]–[71], even slight differences in the target current densities might decide on the tES treatment to take effect or not. In this context, the presented data indicates that it is important to consider the targeting of the electric field (spatial extent and bias), to effectively direct the electric field to the stimulation target.

E. HETEROGENEITY OF ELECTRIC FIELDS ACROSS TARGET ORIENTATIONS

In order to describe the reliability of the targeting methods, we quantified the heterogeneity of electric field intensities and focality of electric fields across the three different target orientations. A reliable method would need flexible handling of the electrode positioning, in order to control the electric field inside the head model with changing target orientation. On average, ADMM showed the least heterogenous results (0.37 ± 0.15 SD), followed by the 5 × 1 control (0.56 ± 0.13 SD) and CMI (0.74 ± 0.22 SD; Fig. 4D). A repeated- measures ANOVA confirmed significant heterogeneity differences between the methods ($F_{1.5,\ 30.2} = 35.25$, $p < .001$, $\eta_p^2 = .64$). Follow-up t-tests revealed significant differences between all three comparisons (ADMM < CMI: $t_{20} = -10.38$, $p < .001$, $r = .92$; ADMM < 5 × 1: $t_{20} = -4.94$, $p < .001$, $r = .74$; CMI > 5 × 1: $t_{20} = 3.22$, $p = .004$, $r = .58$).

In sum, ADMM showed more reliable results across the three different target orientations of the simulated parietal target in the present study, compared to the 5 × 1 control and the CMI in terms of electric field heterogeneity.

Although ADMM restricts the distance of electrode positions to the stimulation target (Fig. 2), it manages to reliably adapt the target intensities and spatial extent of electric fields according to the target orientation, with only slight changes to the electrode positions. CMI likely resulted in the most heterogeneous results, due to its rationale to only control the target intensity, irrespective of the spatial extent of the induced electric fields. As can be seen in Fig. 2 (especially for the radial orientation), CMI makes extensive use of the electrode layout to place the electrodes according to the individual anatomy. This results in overall increased target current densities, but also increased heterogeneity. As can be seen in Fig. 2, for the 5 × 1 control montage, electrodes are not adapted to the stimulation target orientation and the resulting electric fields are highly dependent on the respective anatomical properties and target orientations. Overall, the 5 × 1 control shows more heterogenous results, compared to the ADMM (Fig. 4D; Table 1), reduced alignment of the electric fields to the target orientation (Fig. 3) and, at least partly, strong bias of the electric fields (Fig. 4B, Table 1).

F. TARGET-DEPENDENT, INDIVIDUAL STIMULATION PROFILES

As described previously [34], we observed a trade-off between intensity and focality, when comparing focality-optimizing (ADMM) and intensity-optimizing (CMI) algorithms for targeted tES (Fig. 4A). Both the ADMM and the CMI were not able to reduce the *inter-individual variability* of target intensities on a descriptive level, given that the same current was applied to the electrodes in all montages and head models (Fig. 4A). Instead, the individually optimized target intensities seemed to be limited by the individual anatomical properties of the head model for the given parietal stimulation target.

Across subjects an inverse relationship between intensity and focality was apparent in the present data (Fig. 4C). Some subjects showed higher values of stimulation intensity *and* focality for some CMI and 5 × 1 montages, relative to other subjects. This observation indicates that no within-subject trade-off between target intensity and spatial extent can be held accountable for the inter-subject variability of the electric field properties. The data rather indicate the existence of individual profiles that might determine the potential tES-efficacy for a given stimulation target, solely based on the individual anatomy.

In sum, the *a priori* estimation and the post-hoc evaluation of individual tES-induced target current densities are highly recommended in order to evaluate effects of individual anatomy on the behavioral or neurophysiological efficacy of tES.

Recent studies showed that the stimulation intensity and focality that can be achieved by targeting is strongly dependent on the respective location of the stimulation target within the cortex of *one standard FEM head model* [36], [66]. Critically, the present results further indicate that, in addition, *inter-individual variability* (i.e. across head models) should be considered for each target location, due to the variability that is introduced by individual anatomy.

In this framework, individually targeted tES may improve the control over induced electric fields to raise the probability of tES to take effect. In the present study, ADMM and CMI both exhibited their effect by optimizing the electric field properties with respect to the stimulation target. CMI was able to maximize the target current densities along the target orientation (target intensity) for all target orientations and across subjects. ADMM produced electric fields that were less prone to varying orientations of the target within the individual parietal cortices (heterogeneity; Fig. 4D) compared to CMI and the 5×1 control. In addition, for ADMM the overall smallest bias was observed (Fig. 4B).

IV. CONCLUSION

Individual anatomical properties lead to variability of induced electric fields and thereby to differences in the potential tES efficacy. Targeting of tES electric fields using one of various optimization algorithms [34]–[37], [65], [66] is suitable to increase the level of control over the individual intracranial current densities with respect to target intensities, as well as target orientation and spatial properties of the electric field (bias and spatial extent of electric fields). In the present study, the focality-optimizing ADMM algorithm allowed a balance between spatial extent and target intensity, while flexibly adapting to target orientation and individual anatomy. The intensity-optimizing CMI algorithm increased the target intensities of the individual electric fields, thereby raising the overall chance of a physiological tES effect [76]. The experimental sample size we used, allowed insight into the variance of electric field parameters and the dependency of optimized stimulation montages and electric field properties on the individual anatomy. We show that optimized stimulation target intensity and focality show *variation across inter-individual FEM head models* for the given parietal stimulation target, with respect to target intensities, spatial extent, bias and parallelity of electric fields, as well as across different target orientations (heterogeneity). These results complement recent studies that showed large *variation across cortical regions in one FEM head model* [36], [66]. The simulated electric fields in the present study showed variation in target intensities that indicates differences in the potential efficacy of tES across subjects, given that the same current is applied to all participants. While a correspondence of the tES-induced electric fields and individual neurophysiological [16], [17] and behavioral tES effects seems absolute intuitive, until now this relation lacks of substantial experimental evidence.

In conclusion, FEM simulations of transcranial electric fields and the application of targeted tES might help to increase the physiological interpretability of tES effects. We propose that an algorithmic definition of individual stimulation montages *a priori* and the detailed analysis of estimated electric fields has potential to improve the understanding of mechanisms underlying tES and thus its' effectiveness in future applications.

REFERENCES

[1] J. P. Lefaucheur, "A comprehensive database of published tDCS clinical trials (2005–2016)," *Clin. Neurophysiol.*, vol. 46, no. 6, pp. 319–398, 2016.

[2] D. J. L. G. Schutter and M. Wischnewski, "A meta-analytic study of exogenous oscillatory electric potentials in neuroenhancement," *Neuropsychologia*, vol. 86, pp. 110–118, Jun. 2016.

[3] M. A. Nitsche, L. G. Cohen, E. M. Wassermann, A. Priori, N. Lang, A. Antal, W. Paulus, F. Hummel, P. S. Boggio, F. Fregni, and A. Pascual-Leone, "Transcranial direct current stimulation: State of the art 2008," *Brain Stimulation*, vol. 1, no. 3, pp. 206–223, 2008.

[4] M. A. Nitsche and W. Paulus, "Transcranial direct current stimulation–update 2011," *Restorative Neurol. Neurosci.*, vol. 29, no. 6, pp. 463–492, 2011.

[5] V. López-Alonso, B. Cheeran, D. Río-Rodríguez, and M. Fernández-del-Olmo, "Inter-individual variability in response to non-invasive brain stimulation paradigms," *Brain Stimulation*, vol. 7, no. 3, pp. 372–380, May 2014.

[6] M. R. van Schouwenburg, L. K. A. Sörensen, R. de Klerk, L. C. Reteig, and H. A. Slagter, "No differential effects of two different alpha-band electrical stimulation protocols over fronto-parietal regions on spatial attention," *Frontiers Neurosci.*, vol. 12, pp. 1–12, Jul. 2018.

[7] D. Veniero, C. S. Y. Benwell, M. M. Ahrens, and G. Thut, "Inconsistent effects of parietal α-tACS on pseudoneglect across two experiments: A failed internal replication," *Frontiers Psychol.*, vol. 8, pp. 1–14, Jun. 2017.

[8] D. Veniero, A. Vossen, J. Gross, and G. Thut, "Lasting EEG/MEG aftereffects of rhythmic transcranial brain stimulation: Level of control over oscillatory network activity," *Frontiers Cellular Neurosci.*, vol. 9, p. 477, Dec. 2015.

[9] S. Wiethoff, M. Hamada, and J. C. Rothwell, "Variability in response to transcranial direct current stimulation of the motor cortex," *Brain Stimulation*, vol. 7, no. 3, pp. 468–475, May 2014.

[10] S. Bestmann, A. O. de Berker, and J. Bonaiuto, "Understanding the behavioural consequences of noninvasive brain stimulation," *Trends Cognit. Sci.*, vol. 19, no. 1, pp. 13–20, Jan. 2015.

[11] J. C. Horvath, J. D. Forte, and O. Carter, "Evidence that transcranial direct current stimulation (tDCS) generates little-to-no reliable neurophysiologic effect beyond MEP amplitude modulation in healthy human subjects: A systematic review," *Neuropsychologia*, vol. 66, pp. 213–236, Jan. 2015.

[12] J. C. Horvath, J. D. Forte, and O. Carter, "Quantitative review finds no evidence of cognitive effects in healthy populations from single-session transcranial direct current stimulation (tDCS)," *Brain Stimulation*, vol. 8, no. 3, pp. 535–550, May 2015.

[13] G. Thut, T. O. Bergmann, F. Fröhlich, S. R. Soekadar, J.-S. Brittain, A. Valero-Cabré, A. T. Sack, C. Miniussi, A. Antal, H. R. Siebner, U. Ziemann, and C. S. Herrmann, "Guiding transcranial brain stimulation by EEG/MEG to interact with ongoing brain activity and associated functions: A position paper," *Clin. Neurophysiol.*, vol. 128, no. 5, pp. 843–857, May 2017.

[14] A. Opitz, W. Paulus, S. Will, A. Antunes, and A. Thielscher, "Determinants of the electric field during transcranial direct current stimulation," *NeuroImage*, vol. 109, pp. 140–150, Apr. 2015.

[15] I. Laakso, S. Tanaka, S. Koyama, V. De Santis, and A. Hirata, "Inter-subject variability in electric fields of motor cortical tDCS," *Brain Stimulation*, vol. 8, no. 5, pp. 906–913, Sep. 2015.

[16] L. Johnson, I. Alekseichuk, J. Krieg, A. Doyle, Y. Yu, J. Vitek, M. Johnson, and A. Opitz, "Dose-dependent effects of transcranial alternating current stimulation on spike timing in awake nonhuman primates," *Sci. Adv.*, vol. 6, no. 36, Sep. 2020, Art. no. eaaz2747.

[17] F. H. Kasten, K. Duecker, M. C. Maack, A. Meiser, and C. S. Herrmann, "Integrating electric field modeling and neuroimaging to explain inter-individual variability of tACS effects," *Nature Commun.*, vol. 10, no. 1, p. 5427, Dec. 2019.
[18] A. O. D. Berker, M. Bikson, and S. Bestmann, "Predicting the behavioral impact of transcranial direct current stimulation: Issues and limitations," *Frontiers Human Neurosci.*, vol. 7, pp. 1–6, Oct. 2013.
[19] A. Liu, M. Vöröslakos, G. Kronberg, S. Henin, M. R. Krause, Y. Huang, A. Opitz, A. Mehta, C. C. Pack, B. Krekelberg, A. Berényi, L. C. Parra, L. Melloni, O. Devinsky, and G. Buzsáki, "Immediate neurophysiological effects of transcranial electrical stimulation," *Nature Commun.*, vol. 9, no. 1, pp. 1–12, Dec. 2018.
[20] R. Polanía, M. A. Nitsche, and C. C. Ruff, "Studying and modifying brain function with non-invasive brain stimulation," *Nature Neurosci.*, vol. 21, no. 2, pp. 174–187, Feb. 2018.
[21] D. Q. Truong, G. Magerowski, G. L. Blackburn, M. Bikson, and M. Alonso-Alonso, "Computational modeling of transcranial direct current stimulation (tDCS) in obesity: Impact of head fat and dose guidelines," *NeuroImage, Clin.*, vol. 2, no. 1, pp. 759–766, 2013.
[22] J. P. Dmochowski, A. Datta, Y. Huang, J. D. Richardson, M. Bikson, J. Fridriksson, and L. C. Parra, "Targeted transcranial direct current stimulation for rehabilitation after stroke," *NeuroImage*, vol. 75, pp. 12–19, Jul. 2013.
[23] S. Wagner, S. M. Rampersad, Ü. Aydin, J. Vorwerk, T. F. Oostendorp, T. Neuling, C. S. Herrmann, D. F. Stegeman, and C. H. Wolters, "Investigation of tDCS volume conduction effects in a highly realistic head model," *J. Neural Eng.*, vol. 11, no. 1, Feb. 2014, Art. no. 016002.
[24] Y. Huang, A. A. Liu, B. Lafon, D. Friedman, M. Dayan, X. Wang, M. Bikson, W. K. Doyle, O. Devinsky, and L. C. Parra, "Measurements and models of electric fields in the *in vivo* human brain during transcranial electric stimulation," *eLife*, vol. 6, pp. 1–27, Feb. 2017.
[25] O. D. Creutzfeldt, G. H. Fromm, and H. Kapp, "Influence of transcortical d-c currents on cortical neuronal activity," *Experim. Neurol.*, vol. 5, no. 6, pp. 436–452, Jun. 1962.
[26] M. A. Nitsche and W. Paulus, "Excitability changes induced in the human motor cortex by weak transcranial direct current stimulation," *J. Physiol.*, vol. 527, no. 3, pp. 633–639, Sep. 2000.
[27] T. D. Krieg, F. S. Salinas, S. Narayana, P. T. Fox, and D. J. Mogul, "PET-based confirmation of orientation sensitivity of TMS-induced cortical activation in humans," *Brain Stimulation*, vol. 6, no. 6, pp. 898–904, Nov. 2013.
[28] T. D. Krieg, F. S. Salinas, S. Narayana, P. T. Fox, and D. J. Mogul, "Computational and experimental analysis of TMS-induced electric field vectors critical to neuronal activation," *J. Neural Eng.*, vol. 12, no. 4, Aug. 2015, Art. no. 046014.
[29] T. Radman, R. L. Ramos, J. C. Brumberg, and M. Bikson, "Role of cortical cell type and morphology in subthreshold and suprathreshold uniform electric field stimulation *in vitro*," *Brain Stimulation*, vol. 2, no. 4, pp. 215.e3–228.e3, 2009.
[30] M. Windhoff, A. Opitz, and A. Thielscher, "Electric field calculations in brain stimulation based on finite elements: An optimized processing pipeline for the generation and usage of accurate individual head models," *Hum. Brain Mapping*, vol. 34, no. 4, pp. 923–935, Apr. 2013.
[31] T. Wagner, F. Fregni, S. Fecteau, A. Grodzinsky, M. Zahn, and A. Pascual-Leone, "Transcranial direct current stimulation: A computer-based human model study," *NeuroImage*, vol. 35, no. 3, pp. 1113–1124, Apr. 2007.
[32] A. Datta, V. Bansal, J. Diaz, J. Patel, D. Reato, and M. Bikson, "Gyri-precise head model of transcranial direct current stimulation: Improved spatial focality using a ring electrode versus conventional rectangular pad," *Brain Stimulation*, vol. 2, no. 4, pp. 201.e1–207.e1, Oct. 2009.
[33] S. Wagner, M. Burger, and C. H. Wolters, "An optimization approach for well-targeted transcranial direct current stimulation," *SIAM J. Appl. Math.*, vol. 76, no. 6, pp. 2154–2174, Jan. 2016.
[34] J. P. Dmochowski, A. Datta, M. Bikson, Y. Su, and L. C. Parra, "Optimized multi-electrode stimulation increases focality and intensity at target," *J. Neural Eng.*, vol. 8, no. 4, Aug. 2011, Art. no. 046011.
[35] G. Ruffini, M. D. Fox, O. Ripolles, P. C. Miranda, and A. Pascual-Leone, "Optimization of multifocal transcranial current stimulation for weighted cortical pattern targeting from realistic modeling of electric fields," *NeuroImage*, vol. 89, pp. 216–225, 2014.
[36] J. P. Dmochowski, L. Koessler, A. M. Norcia, M. Bikson, and L. C. Parra, "Optimal use of EEG recordings to target active brain areas with transcranial electrical stimulation," *NeuroImage*, vol. 157, pp. 69–80, Mar. 2017.
[37] S. Guler, M. Dannhauer, B. Erem, R. Macleod, D. Tucker, S. Turovets, P. Luu, D. Erdogmus, and D. H. Brooks, "Optimization of focality and direction in dense electrode array transcranial direct current stimulation (tDCS)," *J. Neural Eng.*, vol. 13, no. 3, Jun. 2016, Art. no. 036020.
[38] C. Göksu, L. G. Hanson, H. R. Siebner, P. Ehses, K. Scheffler, and A. Thielscher, "Human *in-vivo* brain magnetic resonance current density imaging (MRCDI)," *NeuroImage*, vol. 171, pp. 26–39, Dec. 2018.
[39] A. Opitz, A. Falchier, C.-G. Yan, E. M. Yeagle, G. S. Linn, P. Megevand, A. Thielscher, R. Deborah A., M. P. Milham, A. D. Mehta, and C. E. Schroeder, "Spatiotemporal structure of intracranial electric fields induced by transcranial electric stimulation in humans and nonhuman primates," *Sci. Rep.*, vol. 6, no. 1, p. 31236, Nov. 2016.
[40] K. Kar, J. Duijnhouwer, and B. Krekelberg, "Transcranial alternating current stimulation attenuates neuronal adaptation," *J. Neurosci.*, vol. 37, no. 9, pp. 2325–2335, Mar. 2017.
[41] B. Lafon, S. Henin, Y. Huang, D. Friedman, L. Melloni, T. Thesen, W. Doyle, G. Buzsáki, O. Devinsky, L. C. Parra, and A. A. Liu, "Low frequency transcranial electrical stimulation does not entrain sleep rhythms measured by human intracranial recordings," *Nature Commun.*, vol. 8, no. 1, p. 1199, Dec. 2017.
[42] N. M. Boayue, G. Csifcsák, O. Puonti, A. Thielscher, and M. Mittner, "Head models of healthy and depressed adults for simulating the electric fields of non-invasive electric brain stimulation," *FResearch*, vol. 7, p. 704, Nov. 2018.
[43] A. Del Felice, L. Castiglia, E. Formaggio, M. Cattelan, B. Scarpa, P. Manganotti, E. Tenconi, and S. Masiero, "Personalized transcranial alternating current stimulation (tACS) and physical therapy to treat motor and cognitive symptoms in Parkinson's disease: A randomized cross-over trial," *NeuroImage, Clin.*, vol. 22, Jul. 2019, Art. no. 101768.
[44] P. P. Shah-Basak, C. Norise, G. Garcia, J. Torres, O. Faseyitan, and R. H. Hamilton, "Individualized treatment with transcranial direct current stimulation in patients with chronic non-fluent aphasia due to stroke," *Frontiers Hum. Neurosci.*, vol. 9, pp. 1–12, Apr. 2015.
[45] M. E. Mendonca, M. B. Santana, A. F. Baptista, A. Datta, M. Bikson, F. Fregni, and C. P. Araujo, "Transcranial DC stimulation in fibromyalgia: Optimized cortical target supported by high-resolution computational models," *J. Pain*, vol. 12, no. 5, pp. 610–617, May 2011.
[46] D. Edwards, M. Cortes, A. Datta, P. Minhas, E. M. Wassermann, and M. Bikson, "Physiological and modeling evidence for focal transcranial electrical brain stimulation in humans: A basis for high-definition tDCS," *NeuroImage*, vol. 74, pp. 266–275, Jul. 2013.
[47] A. Khan, J. Haueisen, C. H. Wolters, M. Antonakakis, N. Vogenauer, A. Wollbrink, S. Suntrup-Krueger, T. R. Schneider, C. S. Herrmann, M. Nitsche, and W. Paulus, "Constrained maximum intensity optimized multi-electrode tDCS targeting of human somatosensory network," in *Proc. 41st Annu. Int. Conf. IEEE Eng. Med. Biol. Soc. (EMBC)*, Jul. 2019, pp. 2–5.
[48] R. Oostenveld, P. Fries, E. Maris, and J.-M. Schoffelen, "FieldTrip: Open source software for advanced analysis of MEG, EEG, and invasive electrophysiological data," *Comput. Intell. Neurosci.*, vol. 2011, pp. 1–9, Oct. 2011.
[49] G. Nolte. *MEG & EEG Toolbox of Hamburg (METH)*. Accessed: May 13, 2019. [Online]. Available: https://www.uke.de/english/departments-institutes/institutes/neurophysiology-and-pathophysiology/research/working-groups/index.html
[50] SimBio Development Group. *SimBio: A Generic Environment for Bio-Numerical Simulations*. Accessed: Jun. 21, 2018. [Online]. Available: https://www.mrt.uni-jena.de/simbio
[51] Ü. Aydin, J. Vorwerk, P. Küpper, M. Heers, H. Kugel, A. Galka, L. Hamid, J. Wellmer, C. Kellinghaus, S. Rampp, and C. H. Wolters, "Combining EEG and MEG for the reconstruction of epileptic activity using a calibrated realistic volume conductor model," *PLoS ONE*, vol. 9, no. 3, Mar. 2014, Art. no. e93154.
[52] S. Wagner, F. Lucka, J. Vorwerk, C. S. Herrmann, G. Nolte, M. Burger, and C. H. Wolters, "Using reciprocity for relating the simulation of transcranial current stimulation to the EEG forward problem," *NeuroImage*, vol. 140, pp. 163–173, Oct. 2016.
[53] C. H. Wolters, A. Anwander, G. Berti, and U. Hartmann, "Geometry-adapted hexahedral meshes improve accuracy of finite-element-method-Based EEG source analysis," *IEEE Trans. Biomed. Eng.*, vol. 54, no. 8, pp. 1446–1453, Aug. 2007.
[54] J. Ashburner and K. J. Friston, "Unified segmentation," *NeuroImage*, vol. 26, no. 3, pp. 839–851, Jul. 2005.

[55] Y. Huang, J. P. Dmochowski, Y. Su, A. Datta, C. Rorden, and L. C. Parra, "Automated MRI segmentation for individualized modeling of current flow in the human head," *J. Neural Eng.*, vol. 10, no. 6, Dec. 2013, Art. no. 066004.

[56] J. D. Nielsen, K. H. Madsen, O. Puonti, H. R. Siebner, C. Bauer, C. G. Madsen, G. B. Saturnino, and A. Thielscher, "Automatic skull segmentation from MR images for realistic volume conductor models of the head: Assessment of the state-of-the-art," *NeuroImage*, vol. 174, pp. 587–598, Jul. 2018.

[57] J. Vorwerk, C. Engwer, S. Pursiainen, and C. H. Wolters, "A mixed finite element method to solve the EEG forward problem," *IEEE Trans. Med. Imag.*, vol. 36, no. 4, pp. 930–941, Apr. 2017.

[58] C. Engwer, J. Vorwerk, J. Ludewig, and C. H. Wolters, "A discontinuous Galerkin method to solve the EEG forward problem using the subtraction approach," *SIAM J. Sci. Comput.*, vol. 39, no. 1, pp. B138–B164, Jan. 2017.

[59] S. Pursiainen, B. Agsten, S. Wagner, and C. H. Wolters, "Advanced boundary electrode modeling for tES and parallel tES/EEG," *IEEE Trans. Neural Syst. Rehabil. Eng.*, vol. 26, no. 1, pp. 37–44, Jan. 2018.

[60] N. Tzourio-Mazoyer, B. Landeau, D. Papathanassiou, F. Crivello, O. Etard, N. Delcroix, B. Mazoyer, and M. Joliot, "Automated anatomical labeling of activations in SPM using a macroscopic anatomical parcellation of the MNI MRI single-subject brain," *NeuroImage*, vol. 15, no. 1, pp. 273–289, Jan. 2002.

[61] M. Corbetta and G. L. Shulman, "Control of goal-directed and stimulus-driven attention in the brain," *Nat. Rev. Neurosci.*, vol. 3, no. 3, pp. 201–215, Mar. 2002.

[62] M. R. van Schouwenburg, T. P. Zanto, and A. Gazzaley, "Spatial attention and the effects of frontoparietal alpha band stimulation," *Frontiers Hum. Neurosci.*, vol. 10, pp. 1–11, Jan. 2017.

[63] S. Holm, "A simple sequentially rejective multiple test procedure," *Scandin. J. Statist.*, vol. 6, no. 2, pp. 65–70, 1979.

[64] Y. Huang and L. C. Parra, "Can transcranial electric stimulation with multiple electrodes reach deep targets?" *Brain Stimulation*, vol. 12, no. 1, pp. 30–40, Jan. 2019.

[65] S. Rampersad, B. Roig-Solvas, M. Yarossi, P. P. Kulkarni, E. Santarnecchi, A. D. Dorval, and D. H. Brooks, "Prospects for transcranial temporal interference stimulation in humans: A computational study," *NeuroImage*, vol. 202, Nov. 2019, Art. no. 116124.

[66] G. B. Saturnino, H. R. Siebner, A. Thielscher, and K. H. Madsen, "Accessibility of cortical regions to focal TES: Dependence on spatial position, safety, and practical constraints," *NeuroImage*, vol. 203, Dec. 2019, Art. no. 116183.

[67] A. Datta, D. Truong, P. Minhas, L. C. Parra, and M. Bikson, "Inter-individual variation during transcranial direct current stimulation and normalization of dose using MRI-derived computational models," *Frontiers Psychiatry*, vol. 3, p. 91, Oct. 2012.

[68] J. T. Francis, B. J. Gluckman, and S. J. Schiff, "Sensitivity of neurons to weak electric fields," *J. Neurosci.*, vol. 23, no. 19, pp. 7255–7261, Aug. 2003.

[69] F. Fröhlich and D. A. McCormick, "Endogenous electric fields may guide neocortical network activity," *Neuron*, vol. 67, no. 1, pp. 129–143, Jul. 2010.

[70] J. K. Deans, A. D. Powell, and J. G. R. Jefferys, "Sensitivity of coherent oscillations in rat hippocampus to AC electric fields," *J. Physiol.*, vol. 583, no. 2, pp. 555–565, Sep. 2007.

[71] D. Reato, A. Rahman, M. Bikson, and L. C. Parra, "Effects of weak transcranial alternating current stimulation on brain activity—A review of known mechanisms from animal studies," *Frontiers Hum. Neurosci.*, vol. 7, pp. 1–8, Oct. 2013.

[72] Ü. Aydin, S. Rampp, A. Wollbrink, H. Kugel, J.-H. Cho, T. R. Knösche, C. Grova, J. Wellmer, and C. H. Wolters, "Zoomed MRI guided by combined EEG/MEG source analysis: A multimodal approach for optimizing presurgical epilepsy work-up and its application in a multi-focal epilepsy patient case study," *Brain Topography*, vol. 30, no. 4, pp. 417–433, Jul. 2017.

[73] C. Schmidt, S. Wagner, M. Burger, U. V. Rienen, and C. H. Wolters, "Impact of uncertain head tissue conductivity in the optimization of transcranial direct current stimulation for an auditory target," *J. Neural Eng.*, vol. 12, no. 4, Aug. 2015, Art. no. 046028.

[74] T. Neuling, S. Rach, and C. S. Herrmann, "Orchestrating neuronal networks: Sustained after-effects of transcranial alternating current stimulation depend upon brain states," *Frontiers Hum. Neurosci.*, vol. 7, pp. 1–12, Apr. 2013.

[75] S. Alagapan, S. L. Schmidt, J. Lefebvre, E. Hadar, H. W. Shin, and F. Fröhlich, "Modulation of cortical oscillations by low-frequency direct cortical stimulation is state-dependent," *PLoS Biol.*, vol. 14, no. 3, pp. 1–21, 2016.

[76] A. Antal and C. S. Herrmann, "Transcranial alternating current and random noise stimulation: Possible mechanisms," *Neural Plasticity*, vol. 2016, Oct. 2016, Art. no. 3616807.

JAN-OLE RADECKE received the B.Sc. degree in psychology from the University of Bremen, Germany, in 2013, and the M.Sc. degree in neurocognitive psychology from the University of Oldenburg, Germany, in 2016. He is currently pursuing the Ph.D. degree in neurophysiology with the Department of Neurophysiology and Pathophysiology, University Medical Center Hamburg-Eppendorf, Hamburg, Germany.

From 2015 to 2017, he was a Student Research Assistant with the Hannover Medical School, Hannover, Germany. Since 2017, he has been working as a Research Assistant with the Department of Neurophysiology and Pathophysiology, University Medical Center Hamburg-Eppendorf. His research interests include neuromodulation using noninvasive brain stimulation in humans, the relation of rhythmic brain activity, behavior and transcranial electric fields, and multisensory perception and cognitive information processing in patients with a cochlea implant.

ASAD KHAN received the B.Sc. degree in electrical (telecommunication) engineering from the COMSATS Institute of Information Technology, Islamabad, Pakistan, in 2007, and the M.Sc. degree in digital communications from the University of Kiel, Kiel, Germany, in 2011. He is currently pursuing the Ph.D. degree with the Institute for Biomagnetism and Biosignalanalysis (IBB), University of Münster, Münster, Germany.

From 2012 to 2016, he was a Lecturer with the Department of Electrical Engineering, COMSATS Institute of Information Technology. Since 2017, he has been working as a Research Assistant with IBB, University of Münster. His research interests include source analysis using combined EEG and MEG and neuromodulation of neuronal networks of the human brain using noninvasive brain stimulation techniques.

ANDREAS K. ENGEL received the degrees in medicine and philosophy from Saarland University, Homburg, the Technical University of Munich, and Goethe University Frankfurt, Germany, and the Ph.D. (Dr.med.) degree from the Technical University of Munich, in 1987, having completed his medical exams.

From 1987 to 1995, he worked as a Postdoctoral Fellow with Wolf Singer at the Max Planck Institute for Brain Research, Frankfurt, Germany. From 1996 to 2000, he headed a Research Group at the Max Planck Institute for Brain Research which was funded by the Heisenberg Program of the German Research Foundation (DFG). Between Fall 1997 and Summer 1998, he was also affiliated as a Daimler-Benz Fellow with the Institute for Advanced Study, Berlin. From 2000 to 2002, he worked with the Jülich Research Centre as the Head of the Cellular Neurobiology Group, Institute for Medicine. In 2002, he was appointed as the Chair of Neurophysiology with the University Medical Center Hamburg-Eppendorf (UKE), where he has been the Director of the Department of Neurophysiology and Pathophysiology, since 2002. In 2008, he was also elected as a member of the Academy of Sciences and Humanities, Hamburg. Since 2011, he has been the Coordinator of the Collaborative Research Centre SFB 936 (Multi-Site Communication in the Brain, with C. Gerloff, Department of Neurology, UKE).

CARSTEN H. WOLTERS received the M.Sc. degree in mathematics with a minor in medicine from RWTH Aachen University, Aachen, Germany, in 1997, the Ph.D. degree in mathematics from Leipzig University, Leipzig, Germany, in 2003, and the Habilitation degree in mathematics from the University of Münster, Münster, Germany, in 2008.

From 1997 to 2004, he was with the Max Planck Institute for Human Cognitive and Brain Sciences, Leipzig, and the Max Planck Institute for Mathematics in the Sciences, Leipzig. In 2004, he joined the Scientific Computing and Imaging Institute, The University of Utah, Salt Lake City, UT, USA. Since 2005, he has been a Research Associate with the Institute for Biomagnetism and Biosignalanalysis (IBB), University of Münster. Since 2008, he has been heading the research group Stimulation, Imaging and Modeling of NEUROnal networks in the human brain (SIM-NEURO), IBB. Since 2017, he has been a Professor of Neurosciences and Biomedical Engineering. His research interest includes the field of neuroscience with a focus on reconstructing and manipulating neuronal networks in the human brain.

TILL R. SCHNEIDER received the degree in psychology, with a focus on neuropsychology and biopsychology, from Ruhr-University Bochum, Germany, the M.Sc. (Diploma) degree, in 2003, and the Ph.D. (Dr.rer.nat.) degree from the University of Hamburg, Germany, in 2009, investigating oscillatory neuronal activity during multisensory processing.

In 2004, he joined the Department of Neurophysiology and Pathophysiology, University Medical Center Hamburg-Eppendorf, Germany, as a Research Associate. In 2006, he was working with the Donders Institute for Brain, Cognition and Behaviour as a Visiting Scientist. Since 2009, he has been heading the research group Cognitive and Clinical Neurophysiology at the University Medical Center Hamburg-Eppendorf. His research interests include the field of neuronal networks underlying multisensory integration and cognitive processing and modulation of neuronal networks using noninvasive brain stimulation.